Zeitschrift für anorganische und allgemeine Chemie

Journal of Inorganic and General Chemistry
ZAAC
Zeitschrift für anorganische und allgemeine Chemie

RESEARCH ARTICLE OPEN ACCESS

A Mixed Covalent–Supramolecular Interpenetrated Copper–Phosphonate Network

Marcus N. A. Fetzer | Tobias Heinen | Nabil Assahub | Christoph Janiak

Institut für Anorganische Chemie und Strukturchemie, Heinrich-Heine-Universität Düsseldorf, Düsseldorf, Germany

Correspondence: Christoph Janiak (janiak@uni-duesseldorf.de)

Received: 8 April 2026 | **Revised:** 11 May 2026 | **Accepted:** 18 May 2026

Keywords: coordination network | copper | interpenetration | mixed covalent–supramolecular framework | phosphonate

ABSTRACT

A novel copper-based coordination network [Cu(1,4-DPB)(H_2NBP)] was synthesized via a hydrothermal process using 1,4-di(pyridin-4-yl)benzene (1,4-DPB) and naphthalene-1,4-diylbis(hydrogenphosphonate) (H_2NBP^{2-}) as organic linkers. Single-crystal structure analysis shows that the Cu(II) center exhibits a square-planar coordination and is surrounded by three oxygen atoms from different hydrogenphosphonate groups as well as a nitrogen atom from the 1,4-DPB linker. The structure is based on zigzag-shaped Cu–bisphosphonate double strands that are connected by the organic linkers to form a two-dimensional coordination network. These layers are organized via hydrogen bonds into a three-dimensional, two-fold interpenetrated hydrogen-bonded framework as a mixed covalent–supramolecular copper–phosphonate network. Thermogravimetric studies reveal a higher thermal stability of the network compared to the free linkers. Photophysical measurements demonstrate complete quenching of the free linker luminescence upon metal coordination in the network.

1 | Introduction

Phosphonate-based linkers are of continuous interest in materials chemistry and coordination chemistry due to their remarkable ability to form stable and versatile coordination bonds with a wide variety of metal ions [1–4]. In contrast to carboxylate linkers in prototypical metal–organic frameworks (MOFs), phosphonic acid derivatives are characterized by significantly higher coordination flexibility, which stems from their diprotic nature and the possibility of forming two different deprotonation states. Depending on pH, reaction conditions, and metal center, phosphonate groups can adopt mono-, bi-, or tridentate coordination configurations [5]. This structural diversity opens the door to a wide range of coordination polymers [6–13] and MOFs [14–18]. A key characteristic of phosphonate-based materials is their significantly increased chemical, thermal, and hydrolytic stability compared to comparable metal-carboxylate compounds [19, 20]. This stability results primarily from the formation of strong metal–phosphonate (M–O–P) bonds, which confer high resistance to external influences such as moisture, temperature, or chemical stress on the resulting materials. Consequently, phosphonate-based networks are particularly suitable for applications under demanding conditions. Such materials are therefore attracting increasing interest in fields such as catalysis [21–27], ion exchange [28, 29], luminescence [30–36], as well as in functional materials for electrochemical applications, for example, as electrode materials [37–43] or in proton conductivity [44–52]. Beyond these promising properties, the targeted structural prediction and synthesis of phosphonate-based coordination networks remains a significant challenge. A major limiting factor is the sharp decrease in the solubility of the corresponding linker molecules with increasing number of phosphonic acid groups, which considerably complicates the control of nucleation and crystal growth [53]. Furthermore, the comparatively strong M–O–P interactions lead to limited reversibility in the bond formation between metal and phosphonate. However,

Dedicated to Prof. Dr. Peter Klüfers on the Occasion of his 75th Birthday.

This is an open access article under the terms of the Creative Commons Attribution License, which permits use, distribution and reproduction in any medium, provided the original work is properly cited.

© 2026 The Author(s). Zeitschrift für anorganische und allgemeine Chemie published by Wiley-VCH GmbH.

this reversibility is a crucial prerequisite for the formation of well-defined crystalline phases. Consequently, amorphous or nanocrystalline materials are frequently formed, whose structural characterization is difficult and often only possible to a limited extent [54, 55]. These aspects contribute significantly to the fact that the development of new phosphonate-based materials continues to involve a high experimental effort. Linker systems with different functionalities can be used to control network formation more specifically. By combining phosphonate-containing ligands with additional functional groups or by using a second, differently functionalized linker, coordination chemistry can be specifically modulated. For example, nitrogen-containing ligands not only exhibit targeted coordination with the metal centers but, due to their basic character, also significantly influence the degree of deprotonation of the phosphonic acid groups during synthesis. This enables finely tuned control of the local coordination environment as well as the resulting network topology [56–58].

In this article, we describe the synthesis and structural properties of a new copper-based coordination network, [Cu(1,4-DPB)(H_2NBP)] **1**, formed by the linker molecules 1,4-di(pyridin-4-yl)benzene (1,4-DPB) and naphthalene-1,4-diylbis(hydrogenphosphonate) (H_2NBP^{2-}).

2 | Results and Discussion

For the synthesis of compound [Cu(1,4-DPB)(H_2NBP)] (**1**) both 1,4-di(pyridin-4-yl)benzene (1,4-DPB) and naphthalene-1,4-diylbis (phosphonic acid) (H_4NBP) were used as organic linkers (Figures S1–S3). The linker H_4NBP was synthesized using a method established in our group which employs nickel bromide ($NiBr_2$) as a catalyst and subsequently deprotects the intermediate tetraethyl naphthalene-1,4-diylbis(phosphonate) in concentrated hydrochloric acid (Scheme 1) [59].

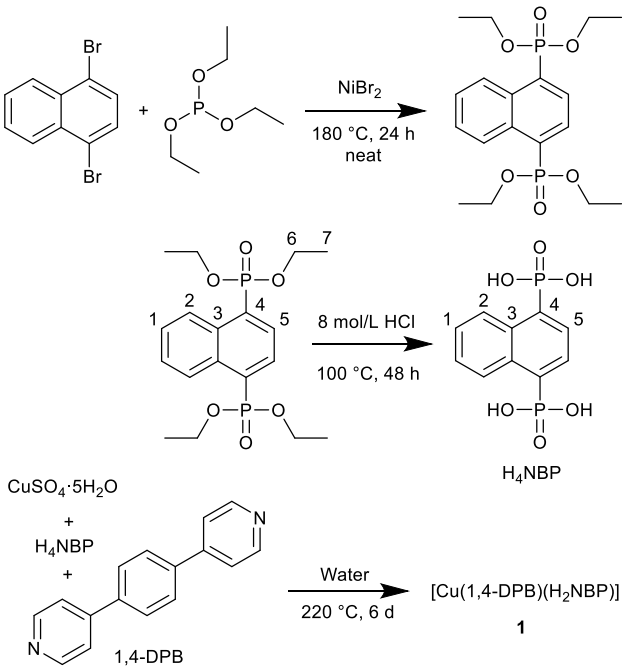

SCHEME 1 | Synthesis of the phosphonate linker H_4NBP and the coordination network **1**. The atom numbering at tetraethyl naphthalene-1,4-diylbis(phosphonate) and H_4NBP is for the NMR spectral assignment in the Experimental Section.

Compound [Cu(1,4-DPB)(H_2NBP)] was then obtained by means of a hydrothermal synthesis. For this purpose, $CuSO_4{\cdot}5H_2O$, 1,4-DPB, and H_4NBP were reacted in ultrapure water to form turquoise crystals (see Section S1). The reaction had to be run with an excess of H_4NBP over 1,4-DPB. Aryl phosphonic acids have typically pK_{a1} values between 1.1 and 2.3 and pK_{a2} between 5.3 and 7.2. The singly deprotonated monohydrogenphosphonate group presents a weak acid whose degree of protolysis increases with decreasing concentration. For the formation of **1** with the H_2NBP^{2-} ligand having monohydrogenphosphonate groups, the formation of fully deprotonated phosphonate groups is counterproductive and will instead lead to different products. A lower excess of the H_4NBP ligand translates into a lower concentration and vice versa. Thus, the higher excess of H_4NBP limits the protolysis of the second deprotonation step. An equimolar setup of 1,4-DPB and H_4NBP, albeit present as such in the formula, did not lead to a defined phase.

The experimentally recorded powder X-ray diffraction (PXRD) pattern of the reaction product in Figure 1 shows significant differences from the used starting materials. No characteristic reflections of the starting compounds, were detected in the obtained product, suggesting that no starting materials were present anymore in crystalline form. Instead, the observed reflections can be fully attributed to the simulated diffractogram from the subsequently determined single-crystal X-ray structure of [Cu(1,4-DPB)(H_2NBP)]. The absence of secondary phases or residual reactants in the PXRD pattern indicates the crystal phase purity of the product. This interpretation is further supported by a matching elemental analysis. The calculated and measured values (see Experimental Section and Table S1) agree well.

Figure 2 depicts the extended asymmetric unit of **1**. The Cu atom is square-planar coordinated by three oxygen atoms from hydrogenphosphonate groups of three different naphthalene-1,4-bis

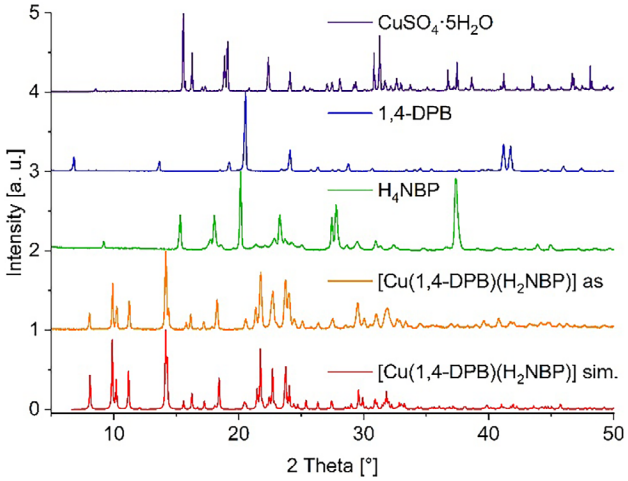

FIGURE 1 | PXRD of the as-synthesized (as) coordination network [Cu(1,4-DPB)(H_2NBP)] and the starting materials, along with the simulation from single-crystal X-ray diffraction.

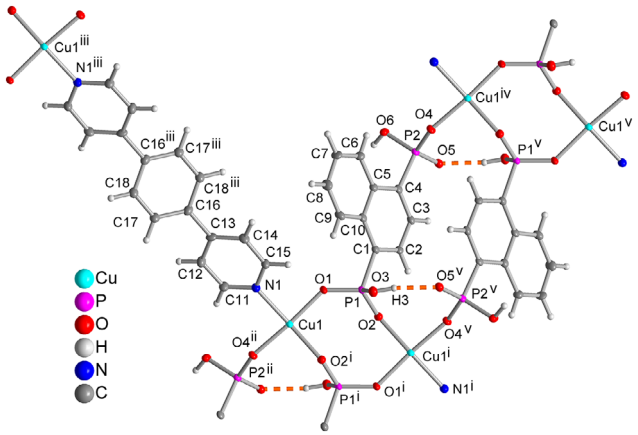

FIGURE 2 | Extended asymmetric unit of **1** (50% thermal ellipsoids, H atoms with arbitrary radii). Intra-strand O(3)–H···O(5) hydrogen bonds are given as dashed orange lines (cf., Table 1). Selected bond lengths and angles are collected in Table S2b. Symmetry codes: (i) $-x+1$, $-y$, $-z+2$; (ii) x, y, $z+1$; (iii) $-x$, $-y+2$, $-z+2$; (iv) x, y, $z-1$; (v) $-x+1$, $-y$, $-z+1$.

(hydrogenphosphonate) linkers and a nitrogen atom from the 1,4-di(pyridin-4-yl)benzene linker. A Continuous Shape Measure (CShM) analysis of the coordination sphere of the Cu atom was performed with the SHAPE V2.1 software [60]. Complex **1** shows an only slightly distorted square-planar configuration based on the shape measure parameter S(square) = 1.30, S(tetrahedron) = 23.40, S(seesaw) = 12.04, S(trigonal bipyramid with vacant axial ligand) = 25.16 (the values for each ideal geometry are 0.00).

Each phosphonate group in the linker is only singly deprotonated, forming a hydrogenphosphonate ($-PO_3H^-$) group. The P–O(H) bond lengths are slightly longer (1.57 Å) than the coordinating P–O bond lengths (~1.51 Å) in line with the formal single bond in P–O(H) and the delocalized formal double bond in the O=P–O^- moiety.

Single deprotonation of a phosphonate group is not uncommon and was also seen in the molecular copper structure of 5-ammonium-1-hydroxypentylidene-1,1-bis(hydrogenphosphonate) and the 2D zinc structure of 3-ammonium-1-hydroxypropylidene-1,1-bis(hydrogenphosphonate) [1], and in the structures of the 3D networks $[La_2(H_5L^1)_2(H_2O)_6]$ (H_8L^1 = 1,3,5,7-tetrakis(4-phenylphosphonic acid)adamantane) [7], $\{[Eu(H_2L_2)_{1.5}(H_2O)_4]\cdot H_2O\}$, and $\{[Ln(H_2L_2)_{1.5}(H_2O)]\cdot H_2O\}$ (Ln = Eu, Gd, Er) (H_4L = diamantane-4,9-bisphosphonic acid) [13].

In the structure of **1**, two inversion-symmetry-related copper atoms are bridged by two hydrogenphosphonate groups forming an eight-membered $(Cu–O–P(1)–O)_2$ metal-phosphonate ring. Thereby this bridging hydrogenphosphonate group with P(1) uses two of its oxygen atoms for metal coordination. Its P–OH group is not involved in the Cu coordination, but forms an intra-strand O(3)–H···O(5) hydrogen-bonding interaction (Figure 2 and Table 1).

The other $-PO_3H^-$ group with P(2) coordinates only with one O atom (namely, O(4)) toward Cu. The second terminal O(5) atom receives the O(3)–H···O(5) intrastrand hydrogen bond and the P(2)–O(6)H group is responsible for the inter-layer hydrogen bonding (see below).

The metal-linker network structure can be constructed from zig-zag Cu–bisphosphonate double strands which run along the *c*-direction and which are connected by the neutral 1,4-DPB linkers to covalent 2D Cu–bisphosphonate–dipyridine layers (Figure 3). These 2D Cu–bisphosphonate–dipyridine layers are then joined to a three-dimensional mixed covalent–hydrogen-bonded or covalent–supramolecular framework [61–64] through complementary hydrogen bonding between P(2)–O(6)H···O(5)–P(2) (Figure 4, Table 1). The PO_3H^- groups with P(2) from two layers

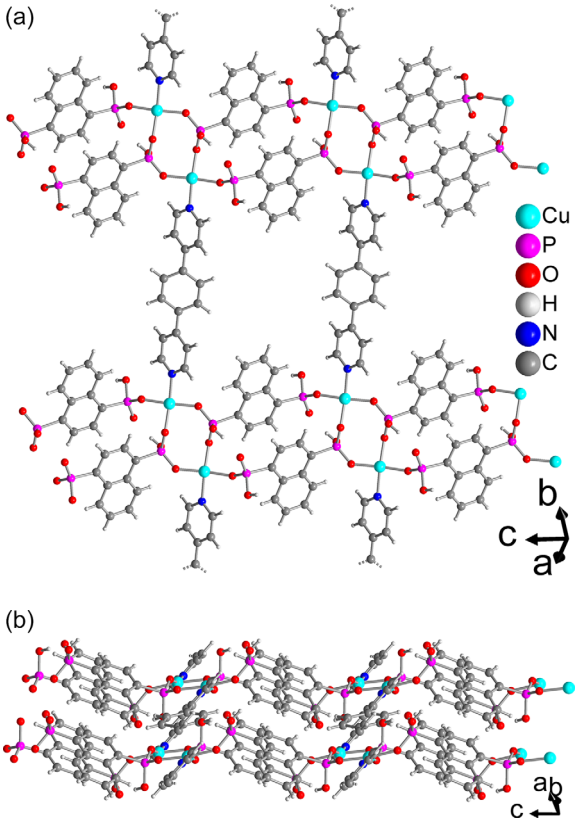

FIGURE 3 | 2D layer in the structure of **1**, viewed (a) perpendicular and (b) approximately along the layer plane to depict the zigzag Cu–bisphosphonate double strands.

TABLE 1 | Parameters of the H-bond interactions in the structure of 1.

D—H···A[a]	D—H, Å	H···A, Å	D···A, Å	D—H···A, °
O3—H3···O5^{v}	0.84	1.80	2.633 (2)	172
O6—H6···O5^{vi}	0.84	1.77	2.610 (2)	176

[a]Symmetry codes: (v) $-x+1$, $-y$, $-z+1$; (vi) $-x$, $-y$, $-z+1$.

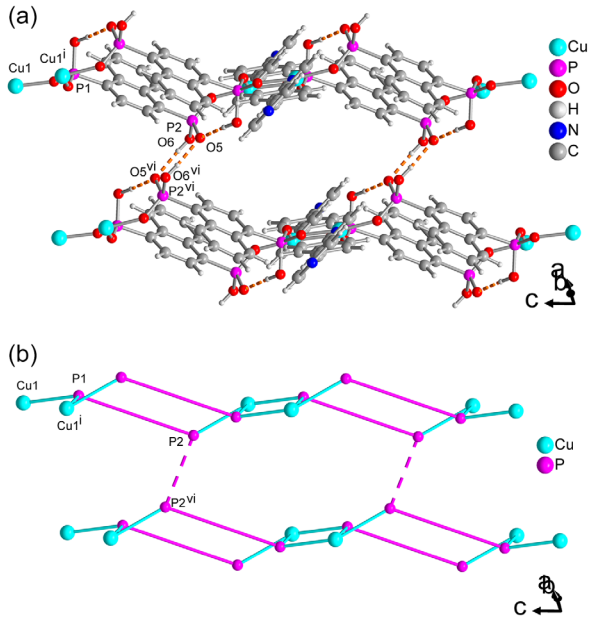

FIGURE 4 | (a) Ball-and-stick presentation of the 3D mixed covalent–supramolecular framework of **1** with the complementary P(2)–O(6)H···O(5)–P(2) hydrogen bonding (dashed orange lines) between the layers in the $R_2^2(8)$ bis-phosphonate rings (Table 1). (b) Schematic framework by retaining only the Cu and P atoms with their topological connectivity and the interlayer $R_2^2(8)$ ring given as a single dashed line. Symmetry codes (i) $-x+1, -y, -z+2$; (vi) $= -x, -y, -z+1$. The two hydrogen-bonded layers presented here in Figure 4 correspond only to one of the interpenetrating nets which are depicted in Figures 5 and S5b as either red or green.

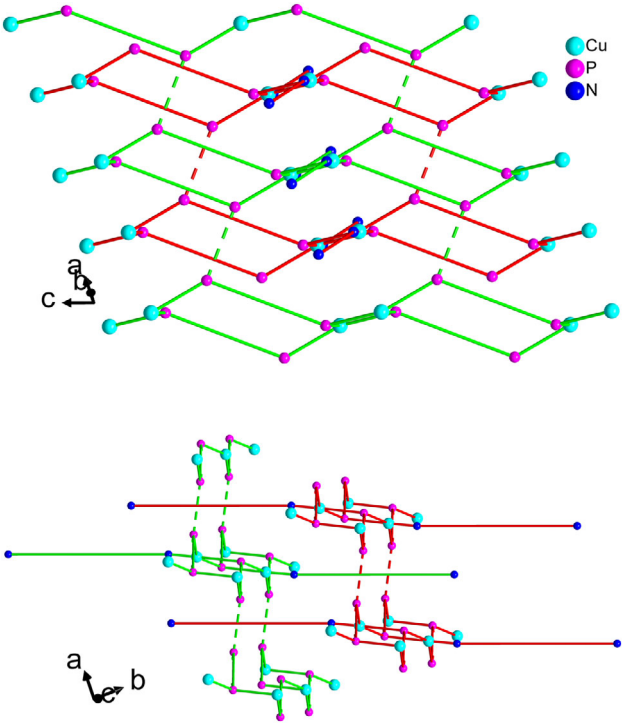

FIGURE 5 | Schematic presentation of the two-fold interpenetration of the symmetry-related 3D mixed covalent–supramolecular frameworks in the packing of **1**, shown in two viewing directions. The frameworks are presented by retaining only the Cu, N, and P atoms with their topological connectivity and the interlayer $R_2^2(8)$ ring given as a dashed line. The two 3D frameworks are differentiated by green and red connections. A ball-and-stick presentation of the interpenetrating frameworks is given in Figure S5b. There are no covalent or hydrogen bonds between the two differently colored frameworks.

form homodimeric $R_2^2(8)$ rings as described by Etter's notation [65–67]. In the Etter symbolism $G_d^a(n)$, the letter *G* encodes the motif (R = ring, C = chain, D = dimer or other finite set, S = intramolecular interaction), the subscript *d* gives the number of hydrogen-bond donors, the superscript *a* gives the number of hydrogen-bond acceptors, and the number *n* in parentheses gives the number of atoms involved in the motif. The hydrogen-bonded $R_2^2(8)$ bis-hydrogenphosphonate ring is identical to the $R_2^2(8)$ ring for carboxylic acids.

The interlayer hydrogen bonding, which is shown in Figure 4, creates channels with rather large rhombic cross sections of about 6 × 4 Å between the van der Waals surfaces (Figure S5a). These channels are filled by the 1,4-di(pyridin-4-yl)benzene (1,4-DPB) linkers of a symmetry related framework, as depicted in Figure 5, giving a two-fold interpenetration. Overall, the structure of **1** represents an interpenetrated three-dimensional hydrogen-bonded network from two-dimensional metal-ligand coordination networks.

A network topology analysis with the TopCryst system [68] using ToposPro algorithms [69] yielded a two-dimensional sql (square lattice) network when the center of the eight-membered $Cu_2(O_2P)_2$ rings was taken as nodes and only the valence bonded connectivity (no hydrogen bonds) was considered. An analysis with ToposPro (Version 5.5.4.1), which includes the H-bonds by taking Cu, P1, and P2 as nodes, gives the point symbol $\{3.4.5.8^2.9\}\{3^2.4^3.5^3.6.7\}\{3^3.4^3.5^3.6\}$ for the 3-nodal net and a $4,5^2$-c net with stoichiometry (4-c)(5-c)(5-c). The structure is correctly analyzed as a 3D framework and two interpenetrating nets.

The supramolecular analysis for possible π–π, C–H–π and C–H···O interactions was carried out with the program PLATON [70]. The PLATON-listing "Analysis of Short Ring-Interactions" for possible π-stacking interactions yielded a single π-stacking contact in the packing of **1** (Figure S5c) which falls into "strong" π-stacking interactions with rather short centroid–centroid contacts (smaller than 3.8 Å), near parallel ring planes (alpha <10° to ~0° or even exactly 0° by symmetry), small slip angles (β, γ <25°), and vertical displacements (slippage <1.5 Å) which translate into a sizable overlap of the aryl-plane areas [71, 72]. All other centroid–centroid contacts are over 4.0 Å. A single and rather long C–H···π(centroid) or perpendicular H-plane contact of 2.85 Å or 2.82 Å, respectively, is found while significant C–H···π contacts start below around 2.7 Å for the (C–)H···ring centroid distances with H-perp also starting below 2.6–2.7 Å and C–H··Cg > 145° [73, 74]. All seven C–H···O interactions are within the extended asymmetric unit (Figure S5d). Hence, the complementary interlayer hydrogen bonding between P(2)–O(6)H···O(5)–P(2) is responsible for organizing the 3D framework and interpenetration.

The infrared (IR) spectrum of the coordination network shows a distinct band at approximately 3430 cm^{-1}, which is already present in the spectra of both linkers and can be attributed to the aromatic C–H valence vibrations (see Section S3). In addition, a band at approximately 2850 cm^{-1} can be attributed primarily to the H_2NBP^{2-} linker. This band is characteristic of O–H valence

vibrations of the phosphonic acid groups. The presence of this vibration in the coordination network indicates that the phosphonic acid groups are not fully deprotonated. At the same time, the reduced intensity of this band compared to the free linker supports a partial deprotonation as derived from the crystal structure. In the range of 1620–1400 cm^{-1}, characteristic bands are observed that can be attributed to the C═C and C═N vibrations of the aromatic and heteroaromatic systems, respectively. Additionally, bands are observable in the region around 1200 cm^{-1} that are typical of P–O and P═O vibrations and indicate the presence of the phosphonate functionality.

To evaluate the thermal stability of **1**, thermogravimetric analyses (TGA) were performed in the temperature range from 125°C to 1000°C. The coordination network exhibits significantly increased thermal stability compared to the free organic linkers (Figure 6).

While the free linkers, H_4NBP and 1,4-DPB, exhibit decomposition processes beginning at approximately 255°C and 190°C, respectively, the thermal decomposition of the covalent–supramolecular framework does not begin to degrade until a significantly higher temperature of approximately 375°C. Sublimation of 1,4-DPB was ruled out by its observing blackening upon heating to 280°C in a melting point tube. In the high-temperature range, a significant residual mass of 45.6% remains, which is close to the theoretical percentage for copper metaphosphate $Cu(PO_3)_2$ (47.5%).

Due to the aromatic structure of the linker molecules used, we investigated the photophysical luminescence properties of the free linkers as well as those of complex **1**. The measurements were performed in the solid state at room temperature in a reflective setup. The spectra in Figure S6 show that both free linkers 1,4-DPB and H_4NBP exhibit significant luminescence in the solid state, which is attributable to their conjugated π-systems. In contrast, no significant luminescence could be detected for complex **1** under identical measurement conditions. The absence of any emission in **1** can be attributed to quenching of the luminescence by the paramagnetic copper atoms, as well as by linker interactions which promote nonradiative channels, leading to the suppression of luminescence.

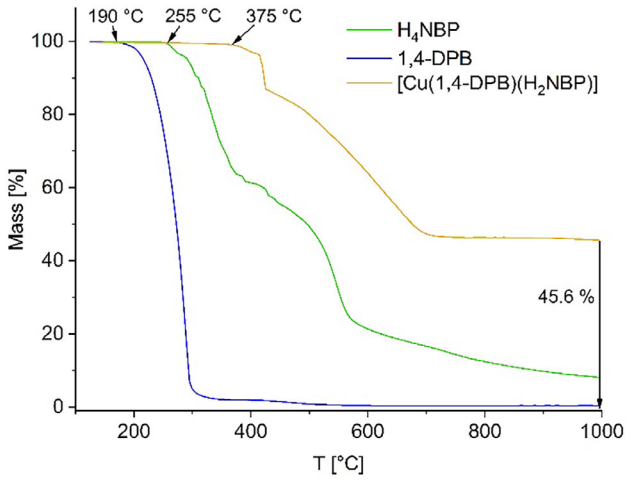

FIGURE 6 | Thermogravimetric determination of the decomposition temperature of the free linkers and the framework **1** in the range from 125°C to 1000°C. The decomposition was carried out at a heating rate of 10 K/min in synthetic air.

3 | Conclusions

In this work, a new copper-based coordination network, [Cu(1,4-DPB)(H_2NBP)], was successfully synthesized under hydrothermal conditions and comprehensively characterized. The combination of PXRD, elemental analysis, and IR spectroscopy confirms the phase purity as well as the successful integration of both organic linkers with partial deprotonation of the phosphonate groups. Single-crystal structure analysis reveals a square-planar coordinated Cu(II) center linked via hydrogenphosphonate groups and pyridine nitrogen atoms. The resulting architecture consists of one-dimensional Cu–bisphosphonate double strands connected by the 1,4-DPB linkers to two-dimensional layers, which are further organized into a three-dimensional, doubly interpenetrated supramolecular framework. Compared to the free linkers, the compound exhibits significantly increased thermal stability. At the same time, the free linker luminescence is completely suppressed due to efficient nonradiative processes. Overall, the results highlight the potential of phosphonate-based ligands for the construction of complex, stable, and structurally versatile coordination networks with additional supramolecular organization.

4 | Experimental Section

4.1 | Chemicals

All chemicals used were purchased commercially from BLDpharm, Carl Roth, Alfa Aesar, Thermo Scientific and TCI and used without further purification.

4.2 | PXRD

PXRD patterns were measured using a Rigaku MiniFlex diffractometer (600 W, 40 kV, 15 mA) with Cu Kα radiation (λ = 1.54182 Å) between $2° < 2\theta < 50°$ at room temperature.

4.3 | TGA

TGAs were performed on a Netzsch TG209 in a synthetic air atmosphere with a ramp of 10 K min^{-1} in a range between 30°C and 1000°C.

4.4 | Fourier Transform Infrared Spectroscopy

Fourier transform infrared spectroscopy (FT-IR) measurements were performed on a Bruker TENSOR 37 IR spectrometer with KBr pellets in the range 500–4000 cm^{-1} at room temperature (Figure S4).

4.5 | Single-Crystal X-Ray Analysis

Single-crystal XRD data were collected at 100 K on a Rigaku XtaLAB Synergy S diffractometer (Rigaku, Tokyo, Japan) equipped with a PhotonJet Cu Kα radiation source ($\lambda = 1.54184$ Å) and a hybrid pixel array detector. Suitable single crystals were selected under a polarized-light Leica M80 microscope (Leica, Wetzlar, Germany) and mounted in oil on a cryo-loop. Data processing, including unit-cell refinement, data reduction, and absorption correction, was carried out with CrysAlisPro [75]. Structures were solved and refined in Olex2 using SHELXT and SHELXL, respectively [76–78]. Structure graphics were generated using the Diamond 5 software [79]. The crystallographic data for the structure are given in Table S2a and were deposited with the Cambridge Crystallographic Data Centre (CCDC deposition number 2544596) and can be obtained free of charge via www.ccdc.cam.ac.uk/data_request/cif [80].

4.6 | Fluorescence Spectroscopy

Fluorescence spectroscopy was carried out using a reflective setup in an FS5 photoluminescence spectrometer (Edinburgh Instruments, Livingston, UK) equipped with a 450 W Xe arc lamp. The solid samples were placed in a brass sample holder. All measurements were performed in ambient air at 293 K.

4.7 | Synthesis of tetraethyl naphthalene-1,4-diylbis(phosphonate)

Under a nitrogen flow, 1,4-dibromonaphthalene (5.1 g, 17.8 mmol) was placed in a three-neck round-bottom flask equipped with a stirring bar. The flask was heated to 160°C to melt the 1,4 dibromonaphthalene. To the molten 1,4-dibromonaphthalene, $NiBr_2$ (0.5 g, 2.2 mmol) was added. Finally, triethyl phosphite (7.8 g, 46.9 mmol) was added dropwise over a period of 7 h. The reaction was continued to be stirred at 160°C for 24 h. The crude product, a dark brown to orange oil, was purified by column chromatography using a mixture of EtOAc and EtOH (9:1 v:v). The product was isolated as a colorless oil with a yield of 3.8 g (9.5 mmol, 53%).

^{1}H NMR (300 MHz, $CDCl_3$) δ 8.63-8.59 (m, 2H, H-5), 8.29-8.22 (m, 2H, H-2), 7.68-7.64 (m, 2H, H-1), 4.27-4.07 (m, 8H, H-6), 1.32 (t, $J = 7.1$ Hz, 12H, H-7); ^{31}P{^{1}H} NMR (121 MHz, $CDCl_3$) δ 17.4 (s); ^{13}C{^{1}H} NMR (75 MHz, $CDCl_3$) δ 132.9-132.4 (imposition of signals of two carbon atoms, C-3), 131.6 (d, $J = 3.6$ Hz, C-4), 129.2 (d, $J = 3.5$ Hz, C-5), 127.6 (s, C-2), 127.3 (s, C-1), 62.5 (d, $J = 3.0$ Hz, C-6), 16.3 (s, C-7) (see Scheme 1 for the atom numbering).

4.8 | Synthesis of naphthalene-1,4-diylbis(phosphonic acid) (H_4NBP)

Tetraethyl naphthalene-1,4-diylbis(phosphonate) (3.8 g, 9.5 mmol) was mixed with 100 mL of 8 mol/L hydrochloric acid and refluxed for 48 h. The white precipitate was filtered off and dried at 60°C under reduced pressure to obtain 2.5 g (yield: 95%) of the acid.

^{1}H NMR (300 MHz, DMSO-d_6) δ 8.69-8.65 (m, 2H, H-5), 8.08-8.01 (m, 2H, H-2), 7.64 (dd, $J = 6.5$, 3.4 Hz, 2H, H-1); ^{31}P{^{1}H} NMR (121 MHz, DMSO-d_6) δ 11.0 (s); ^{13}C{^{1}H} NMR (75 MHz, DMSO-d_6) δ 135.6 (d, $J = 159.0$ Hz, C-4), 132.4 (d, $J = 11.0$ Hz, C-5), 130.3-129.9 (m, C-3), 127.8 (s, C-2), 126.4 (s, C-1). (see Scheme 1 for the atom numbering).

4.9 | Synthesis of catena-{[μ-1,4-di(pyridin-4-yl) benzene-κ^{2}N1,N2][μ$_3$-naphthalene-1,4-diylbis (hydrogenphosphonate)-κ^{3}O1:O2:O4]copper(II)}, [Cu(1,4-DPB)(H_2NBP)] (1)

In a solvothermal reaction $CuSO_4 \cdot 5H_2O$ (150 mg, 0.601 mmol), 1,4-di(pyridin-4-yl)benzene (25 mg, 0.11 mmol), and naphthalene-1,4-diylbis(phosphonic acid) (100 mg, 0.347 mmol) were placed in a Teflon liner for a stainless-steel autoclave and suspended in 10 mL of ultrapure water. The liner was then placed in the autoclave, sealed, and heated for 6 days at 220°C. Then, the system was cooled to room temperature under ambient cooling. Turquoise crystals were separated by filtration, washed 3 times with ultrapure water (3 × 10 mL) and acetone (3 × 10 mL) to remove unreacted starting materials, and then dried under vacuum at 60°C. Yield: 62 mg or 62% based on 1,4-di(pyridin-4-yl)benzene. $C_{18}H_{14}CuNO_6P_2$ calculated C 46.45, H 3.03, N 3.01, found C 46.42, H 2.99, N 2.93%.

Acknowledgments

We thank the Center for Molecular and Structural Analytics at Heinrich Heine University (CeMSA@HHU) for recording the NMR spectra.

Open Access funding enabled and organized by Projekt DEAL.

Conflicts of Interest

The authors declare no conflicts of interest.

Data Availability Statement

The data that support the findings of this study are openly available in Cambridge Crystallographic Data Centre at https://www.ccdc.cam.ac.uk/data_request/cif, reference number 2544596.

References

1. H. A. Habib, B. Gil-Hernández, K. Abu-Shandi, J. Sanchiz, and C. Janiak, "Iron, Copper and Zinc Ammonium-1-Hydroxyalkylidene-Diphosphonates with Zero-, One- and Two-Dimensional Covalent Metal–ligand Structures Extended into Three-Dimensional Supramolecular Networks by Charge-Assisted Hydrogen-Bonding," *Polyhedron* 29 (2010): 2537–2545.

2. N. Plesu, L. Crisan, B. Maranescu, A. Popa, and A. Visa, "Exploring Corrosion Protection with Greener Synthesized Metal Phosphonates," *Sustainable Chemistry and Pharmacy* 44 (2025): 101970.

3. A. Goldman, B. Git-Hernández, S. Milian, et al., "Flexible Bifunctional Monoethylphosphonate/Carboxylates of Zn(Ii) and Co(Ii) Reinforced with DABCO Co-Ligand: Paradigmatic Structural Organization with **Pcu** Topology," *CrystEngComm* 22 (2020): 2933–2944.

4. J. G. Jia, S. S. Bao, G. K. H. Shimizu, and L. M. Zheng, "Layered Metal Phosphonates: Structures and Properties," *Coordination Chemistry Reviews* 534 (2025): 216558.

5. D. Sahoo, R. Suriyanarayanan, and V. Chandrasekhar, "Di-, Tri- and Tetranuclear Molecular Vanadium Phosphonates: A Chloride Encapsulated Tetranuclear Bowl," *Dalton Transactions* 43 (2014): 10898–10909.

6. K. Abu-Shandi, H. Winkler, and C. Janiak, "Structure and Mössbauer Study of the First Mixed-Valence Iron Diphosphonate: ^2_∞\rm {Fe^{II/III(H_2O)_2\}{Fe^III/IICl\}_2(4-O_3PC(OH){(CH_2)_4NH_3\}-PO_3)_2O," *Zeitschrift Fur Anorganische Und Allgemeine Chemie* 632 (2006): 629–633.

7. I. Boldog, K. V. Domasevitch, I. A. Baburin, et al., "A Rare Alb-4,8-Cmce Metal–coordination Network Based on Tetrazolate and Phosphonate functionalized 1,3,5,7-Tetraphenyladamantane," *CrystEngComm* 15 (2013): 1235–1243.

8. K. J. Bladek, M. E. Reid, H. Nishihara, F. Akhtar, B. S. Gelfand, and G. K. H. Shimizu, "Microsphere Assemblies via Phosphonate Monoester Coordination Chemistry," *Chemistry – A European Journal* 24 (2018): 1533–1538.

9. B. Ay, R. Takano, T. Ishida, and E. Yildiz, "Tricopper(II)bis(2-((hydrogen Phosphonato)methyl)benzylphosphonate) as a Layered Oxo-Bridged Copper(II) Coordination Polymer: Synthesis, Structure, Magnetic Property, and Catalytic Activity," *Polyhedron* 225 (2022): 116038.

10. D. Zeng, M. Ren, S. S. Bao, and T. Zheng, "Two Three-Dimensional Mixed-Ligated Cobalt Phosphonate Coordination Polymers: Syntheses, Crystal Structures and Magnetic Properties," *Journal of Molecular Structure* 1248 (2022): 131456.

11. M. Boone, F. Artizzu, J. Goura, D. Mara, R. Van Deun, and M. D'hooghe, "Lanthanide Phosphonate Coordination Polymers," *Coordination Chemistry Reviews* 501 (2024): 215525.

12. S. Ondrusová, D. Buzek, J. Hynek, et al., "Magnetism, Mössbauer Spectroscopy, and Proton Conductivity of Coordination Polymers Based on Phosphonate and Phosphinate Linkers," *Journal of Physical Chemistry C* 129 (2025): 15850–15864.

13. T. Müller, P. Ferber, P. M. Roos, N. Assahub, and C. Janiak, "Lanthanide Coordination Networks Based on Diamantane-4,9-Diphosphonic Acid," *Zeitschrift Fur Anorganische Und Allgemeine Chemie* 652 (2026): e202500158.

14. R. K. Mah, B. S. Gelfand, J. M. Taylor, and G. K. H. Shimizu, "Reconciling Order, Stability, and Porosity in Phosphonate Metal–organic Frameworks via HF-Mediated Synthesis," *Inorganic Chemistry Frontiers* 2 (2015): 273–277.

15. M. Glavinovic, J. H. Perras, B. S. Gelfand, J. B. Lin, and G. K. H. Shimizu, "Orthogonalization of Polyaryl Linkers as a Route to More Porous Phosphonate Metal-Organic Frameworks," *Chemistry – A European Journal* 28 (2022): e202200874.

16. R. P. S. Huynh, D. R. Evans, J. X. Lian, D. Spasyuk, S. Siahrostrami, and G. K. H. Shimizu, "Creating Order in Ultrastable Phosphonate Metal–Organic Frameworks via Isolable Hydrogen-Bonded Intermediates," *Journal of the American Chemical Society* 145 (2023): 21263–21272.

17. M. Glavinovic, J. H. Perras, B. S. Gelfand, et al., "Microporous Metal-Phosphonates with a Novel Orthogonalized Linker and Complementary Guests: Insights for Trivalent Metal Complexes from Divalent Metal Complexes," *Chemistry–A European Journal* 29 (2023): e202203835.

18. R. Serrano-Nieto, S. Carrasco, S. Morales-Cámara, et al., "Novel Pyrene Phosphonate Metal-Organic Frameworks to Efficiently Degrade Sulfamethazine in Wastewater," *Journal of Environmental Chemical Engineering* 13 (2025): 115647.

19. P. Deria, W. Bury, I. Hod, et al., "MOF Functionalization via Solvent-Assisted Ligand Incorporation: Phosphonates Vs Carboxylates," *Inorganic Chemistry* 54 (2015): 2185–2192.

20. A. H. Cao, K. Li, X. Xu, L. T. Kang, and M. Zhang, "The Transformation of a Bimetal Carboxylate-MOF into a Phosphonate-Based MOF as a Multifunctional Photocatalyst," *Inorganic Chemistry Frontiers* 13 (2026): 564–574.

21. J. A. Zhang, Z. Ma, J. Jiao, et al., "Layer-by-Layer Grafting of Titanium Phosphate onto Mesoporous Silica SBA-15 Surfaces: Synthesis, Characterization, and Applications," *Langmuir* 25 (2009): 12541–12549.

22. A. Dutta, J. Mondal, A. K. Patra, and A. Bhaumik, "Synthesis and Temperature-Induced Morphological Control in a Hybrid Porous Iron–Phosphonate Nanomaterial and Its Excellent Catalytic Activity in the Synthesis of Benzimidazoles," *Chemistry – A European Journal* 18 (2012): 13372–13378.

23. P. Bhanja and A. Bhaumik, "Organic–Inorganic Hybrid Metal Phosphonates as Recyclable Heterogeneous Catalysts," *ChemCatChem* 8 (2016): 1607–1616.

24. L. J. Qiu, C. L. Lin, C. Y. Chen, X. Wang, and T. H. Yang, "Synthesis, Crystal Structure and Photocatalytic Properties of Two 2-D Coordination Polymer Constructed from Pyridylmethylphosphonate," *Inorganic Chemistry Communications* 119 (2020): 108123.

25. K. Rathore and R. Jangir, "Insight into Synthesis, Properties and Applications of Metal Phosphonates: Emphasis on Catalytic Activities," *Inorganica Chimica Acta* 559 (2024): 121804.

26. S. R. Zhong, X. L. Xie, T. Huang, and T. Zhang, "Metal–Organic Frameworks with Phosphonate Monoester Linkers for Catalytic C(sp^2)–H Borylation of Alkenes," *Inorganic Chemistry* 64 (2025): 801–806.

27. C. Y. Gao, Y. K. Wu, L. Ding, et al., "A Highly Stable Zinc Phosphonate for Efficient Heterogeneous Catalytic CO2 Cycloaddition and ring-Opening Reaction," *Journal of Environmental Chemical Engineering* 13 (2025): 116468.

28. Y. Zhang, J. D. Wang, P. Apostol, et al., "Bimetallic Anionic Organic Frameworks with Solid-State Cation Conduction for Charge Storage Applications," *Angewandte Chemie International Edition* 62 (2023): e202310033.

29. R. Silbernagel, C. H. Martin, and A. Clearfield, "Zirconium(IV) Phosphonate–Phosphates as Efficient Ion-Exchange Materials," *Inorganic Chemistry* 55 (2016): 1651–1656.

30. I. L. V. Rosa, E. J. Nassar, and O. A. Serra, "Eu3+ and Tb3+ Organophosphonates: Synthesis, Characterization and Luminescent Properties," *Journal of Alloys and Compounds* 275 (1998): 315–317.

31. R. Ferreira, P. Pires, B. de Castro, R. A. S. Ferreira, L. D. Carlos, and U. Pischel, "Zirconium Organophosphonates as Photoactive and Hydrophobic Host Materials for Sensitized Luminescence of Eu (III), Tb (III), Sm (III) and Dy (III)," *New Journal of Chemistry* 28 (2004): 1506–1513.

32. B. H. Yu, Y. J. Wang, M. Y. Sun, Y. Q. Luo, H. R. Yu, and L. Zhang, "Preparation of Carbon Dots-Doped Terbium Phosphonate Coordination Polymers as Ratiometric Fluorescent Probe for Citrate Detection," *Spectrochimica Acta. Part A, Molecular and Biomolecular Spectroscopy* 268 (2022): 120656.

33. Y. T. Zhang, J. X. Ruan, D. S. Ma, J. S. Gao, Y. F. Liu, and Y. H. Yu, "Two Series of Luminescent Phosphonate Coordination Polymers of Lanthanides for Sensing Ketones and Fe3+ in Water," *Polyhedron* 216 (2022): 115694.

34. X. D. Huang, B. K. Hong, G. H. Wen, S. H. Li, and L. M. Zheng, "Photo-Controllable Heterostructured Crystals of Metal–organic Frameworks *via* Reversible Photocycloaddition," *Chemical Science* 14 (2023): 1852–1860.

35. F. Steinke, S. Bette, N. Ruser, et al., "Insights into a New Multi-Stimuli-Responsive Photochromic Metal-Organic Framework: Highly Sensitive Turn-On Luminescence in a Lanthanum Phosphonate," *Advanced Functional Materials* 34 (2024): 2403631.

36. C. Jia, S. Liang, Y. X. Wen, et al., "Photochromic Ln-Phosphonates Assembled by an Imidazole Derivative: Construction, Crystal Structures, and Light-Enhanced Proton Conductivity," *Crystal Growth & Design* 24 (2024): 2202–2209.

37. C. Y. Cheng, S. J. Fu, C. J. Yang, et al., "NCHU-3: A Crystalline Inorganic–Organic Hybrid Molecular Sieve with Extra-Large Cages," *Angewandte Chemie International Edition* 42 (2003): 1937–1940.

38. S. Schmidt, D. Sheptyakov, J. C. Jumas, et al., "Lithium Iron Methylenediphosphonate: A Model Material for New Organic–Inorganic Hybrid Positive Electrode Materials for Li Ion Batteries," *Chemistry of Materials* 27 (2015): 7889–7895.

39. M. Pramanik, Y. Tsujimoto, V. Malgras, S. X. Dou, J. H. Kim, and Y. Yamauchi, "Mesoporous Iron Phosphonate Electrodes with Crystalline Frameworks for Lithium-Ion Batteries," *Chemistry of Material* 27 (2015): 1082–1089.

40. S. M. El-Refaei, P. A. Russo, P. Amsalem, N. Koch, and N. Pinna, "The Importance of Ligand Selection on the Formation of Metal Phosphonate-Derived CoMoP and $CoMoP_2$ Nanoparticles for Catalytic Hydrogen Evolution," *ACS Applied Nano Materials* 3 (2020): 4147–4156.

41. A. Indra, P. W. Menezes, I. Zaharieva, H. Dau, and M. Driess, "Detecting Structural Transformation of Cobalt Phosphonate to Active Bifunctional Catalysts for Electrochemical Water-Splitting," *Journal of Materials Chemistry A* 8 (2020): 2637–2643.

42. P. Salcedo-Abraira, R. Serrano-Nieto, C. Biglione, et al., "Two Cu-Based Phosphonate Metal–Organic Frameworks as Efficient Water-Splitting Photocatalysts," *Chemistry of Materials* 35 (2023): 4211–4219.

43. T. H. Y. Beglau, M. N. A. Fetzer, I. Boldog, et al., "Exceptionally Stable and Super-Efficient Electrocatalysts Derived From Semiconducting Metal Phosphonate Frameworks," *Chemistry – A European Journal* 30 (2024): e202302765.

44. J. M. Taylor, R. K. Mah, I. L. Moudrakovski, C. I. Ratcliffe, R. Vaidhyanathan, and G. K. H. Shimizu, "Facile Proton Conduction via Ordered Water Molecules in a Phosphonate Metal−Organic Framework," *Journal of the American Chemical Society* 132 (2010): 14055–14057.

45. J. M. Taylor, K. W. Dawson, and G. K. H. Shimizu, "A Water-Stable Metal–Organic Framework with Highly Acidic Pores for Proton-Conducting Applications," *Journal of the American Chemical Society* 135 (2013): 1193–1196.

46. Y. S. Wei, X. P. Hu, Z. Han, X. Y. Dong, S. Q. Zang, and T. C. W. Mak, "Unique Proton Dynamics in an Efficient MOF-Based Proton Conductor," *Journal of the American Chemical Society* 139 (2017): 3505–3512.

47. D. A. Levenson, J. F. Zhang, B. S. Gelfand, S. P. Kammampata, V. Thangadurai, and G. K. H. Shimizu, "Particle Size Dependence of Proton Conduction in a Cationic Lanthanum Phosphonate MOF," *Dalton Transactions* 49 (2020): 4022–4029.

48. U. Afrin, M. R. Mian, K. Otake, et al., "Proton Conductivity via Trapped Water in Phosphonate-Based Metal–Organic Frameworks Synthesized in Aqueous Media," *Inorganic Chemistry* 60 (2021): 1086–1091.

49. P. Salcedo-Abraira, C. Biglione, S. M. F. Vilela, et al., "High Proton Conductivity of a Bismuth Phosphonate Metal–Organic Framework with Unusual Topology," *Chemistry of Materials* 35 (2023): 4329–4337.

50. C. Ribeiro, B. W. Tan, F. Figueira, et al., "Mixed Ionic and Electronic Conductivity in a Tetrathiafulvalene-Phosphonate Metal–Organic Framework," *Journal of the American Chemical Society* 147 (2024): 63–68.

51. A. Schmalz, C. G. Eby, C. Moss, B. Bhattacharya, and F. Emmerling, "Thermally Robust 1D Cu(I) Phosphonate Coordination Polymer Exhibiting Enhanced Proton Conductivity via Humidity-Driven Pathways," *Zeitschrift Fur Anorganische Und Allgemeine Chemie* 652 (2026): e202500187.

52. P. M. Ramteke, T. Plechácek, M. Kloda, et al., "Proton-conducting Coordination Polymers Formed from Bipyridine Phosphonate Ligands," *Dalton Transactions* 55 (2026): 5622–5634.

53. C. M. Sevrain, M. Berchel, H. Couthon, and P. A. Jaffrès, "Phosphonic Acid: Preparation and Applications," *Beilstein Journal of Organic Chemistry* 13 (2017): 2186–2213.

54. G. K. H. Shimizu, R. Vaidhyanathan, and J. M. Taylor, "Phosphonate and Sulfonate Metal Organic Frameworks," *Chemical Society Reviews* 38 (2009): 1430–1449.

55. K. J. Gagnon, H. P. Perry, and A. Clearfield, "Conventional and Unconventional Metal–Organic Frameworks Based on Phosphonate Ligands: MOFs and UMOFs," *Chemical Reviews* 112 (2012): 1034–1054.

56. R. Fu, S. Hu, and X. Wu, "New 3D Lanthanide Phosphonates: Syntheses, Crystal Structure, Thermal Stability, Luminescence, and Magnetism," *Crystal Growth & Design* 14 (2014): 6197–6204.

57. A. Bulut, Y. Zorlu, E. Kirpi, et al., "Synthesis of Cu(II)-Organophosphonate Framework with Predefined Void Spaces," *Crystal Growth & Design* 15 (2015): 5665–5669.

58. Y. F. Wei, X. F. Ma, X. D. Huang, G. H. Wen, J. G. Jia, and L. M. Zheng, "Mixed-Ligated Cobalt Phosphonates Showing Slow Magnetic Relaxation and Spin-Flop Behavior," *Journal of Solid State Chemistry* 312 (2022): 123227.

59. R. Oestreich, M. N. A. Fetzer, Y. F. Zhang, et al., "Stable Ultramicroporous Metal–Organic Framework with Hydrophilic and Hydrophobic Domains for Selective Gas Adsorption," *Angewandte Chemie International Edition* 64 (2025): e202513788.

60. M. Llunell, D. Casanova, J. Cirera, P. Alemany, and S. Alvarez, *SHAPE V2.1. Program for the Stereochemical Analysis of Moelcular Fragments by Means of Continuous Shape Measures and Associated Tools* (University of Barcelona, 2013).

61. I. A. Baburin and V. A. Blatov, "Three-Dimensional Hydrogen-Bonded Frameworks in Organic Crystals: A Topological Study," *Acta Crystallographica Section B Structural Science* 63 (2007): 791–802.

62. I. A. Baburin, V. A. Blatov, L. Carlucci, G. Ciani, and D. M. Proserpio, "Interpenetrated Three-Dimensional Hydrogen-Bonded Networks from Metal–organic Molecular and One- or Two-Dimensional Polymeric Motifs," *CrystEngComm* 10 (2008): 1822–1838.

63. I. A. Baburin, "Hydrogen-Bonded Frameworks in Molecular Metal-Organic Crystals: the Network Approach," *Zeitschrift für Kristallographie - Crystalline Materials* 223 (2008): 371–381.

64. I. A. Baburin, V. A. Blatov, L. Carlucci, G. Ciani, and D. M. Proserpio, "Interpenetrated Three-Dimensional Networks of Hydrogen-Bonded Organic Species: A Systematic Analysis of the Cambridge Structural Database," *Crystal Growth & Design* 8 (2008): 519–539.

65. M. C. Etter, "Aggregate Structures of Carboxylic Acids and Amides," *Israel Journal of Chemistry* 25 (1985): 312–319.

66. M. C. Etter, "Encoding and Decoding Hydrogen-Bond Patterns of Organic Compounds," *Accounts of Chemical Research* 23 (1990): 120–126.

67. M. C. Etter, "Hydrogen Bonds as Design Elements in Organic Chemistry," *The Journal of Physical Chemistry* 95 (1991): 4601–4610.

68. A. P. Shevchenko, A. A. Shabalin, I. Yu Karpukhin, and V. A. Blatov, "Topological Representations of Crystal Structures: Generation, Analysis and Implementation in the TopCryst System," *Science and Technology of Advanced Materials: Methods* 2 (2022): 250–265.

69. V. A. Blatov, A. P. Shevchenko, and D. M. Proserpio, "Applied Topological Analysis of Crystal Structures with the Program Package ToposPro," *Crystal Growth & Design* 14 (2014): 3576–3586.

70. A. L. Spek, "Structure Validation in Chemical Crystallography," *Acta Crystallographica Section D: Structural Biology* 65 (2009): 148–155.

71. C. Janiak, "A Critical Account on π–π Stacking in Metal Complexes with Aromatic Nitrogen-Containing Ligands," *Journal of the Chemical Society, Dalton Transactions*. (2000): 3885–3896.

72. X. J. Yang, F. Drepper, B. Wu, W. H. Sun, W. Haehnel, and C. Janiak, "From Model Compounds to Protein Binding: Syntheses, Characterizations and Fluorescence Studies of $[Ru^{II}(bipy)(terpy)L]^{2+}$ Complexes (bipy = 2,2′-Bipyridine; Terpy = 2,2′:6′,2″-Terpyridine; L = Imidazole, Pyrazole and Derivatives, Cytochrome c)," *Dalton Transactions*. (2005): 256–267.

73. O. Takahashi, Y. Kohno, S. Iwasaki, et al., "Hydrogen-Bond-Like Nature of the CH/π Interaction as Evidenced by Crystallographic Database Analyses and Ab Initio Molecular Orbital Calculations," *Bulletin of the Chemical Society of Japan* 74 (2001): 2421–2430.

74. M. Nishio, Y. Umezawa, K. Honda, S. Tsuboyama, and H. Suezawa, "CH/π Hydrogen Bonds in Organic and Organometallic Chemistry," *CrystEngComm* 11 (2009): 1757–1788.

75. CrysAlisPro, *Rigaku Oxford Diffraction, Release 1.171.42.58a* (Agilent; Agilent Technologies Ltd., 2014).

76. O. V. Dolomanov, L. J. Bourhis, R. J. Gildea, J. A. K. Howard, and H. Puschmann, "*OLEX2* : A Complete Structure Solution, Refinement and Analysis Program," *Journal of Applied Crystallography* 42 (2009): 339–341.

77. G. M. Sheldrick, "*SHELXT* – Integrated Space-Group and Crystal-Structure Determination," *Acta Crystallographica Section A Foundations and Advances* 71 (2015): 3–8.

78. G. M. Sheldrick, "Crystal Structure Refinement with *SHELXL*," *Acta Crystallographica Section C Structural Chemistry* 71 (2015): 3–8.

79. K. Brandenburg and H. Putz, *Version 5; Crystal and Molecular Structure Visualization* (Crystal Impact; Gbr, 1997).

80. Deposition number 2544596 contains the supplementary crystallographic data for this paper. These data are provided free of charge by the joint Cambridge Crystallographic Data Centre and Fachinformationszentrum Karlsruhe Access Structures service. www.ccdc.cam.ac.uk/data_request/cif.

Supporting Information

Additional supporting information can be found online in the Supporting Information section.